SUPPORTIVE INFORMATION

MOF-derived Magnetic Microrobots for Active Capture of Nanoplastics

Minitha Cherukutty Ramakrishnan[1], Martin Pumera[1,2,3*]

[1]Future Energy and Innovation Laboratory, Central European Institute of Technology, Brno University of Technology, Purkynova 123, Brno 61200, Czech Republic

[2]Advanced Nanorobots & Multiscale Robotics Laboratory, Faculty of Electrical Engineering and Computer Science, VSB - Technical University of Ostrava, 17. listopadu 2172/15, 70800 Ostrava, Czech Republic

[3]Department of Medical Research, China Medical University Hospital, China Medical University, No. 91 Hsueh-Shih Road, Taichung, Taiwan, China.

✉ *email:* martin.pumera@ceitec.vutbr.cz

Figure S1. FESEM and elemental mapping images of MIL-88(Fe) and its derivatives

Figure S2. FESEM and EDS point analysis for a representative $FeO_x@C_{450^\circ C}$ (MILBots).

Figure S3. FESEM images and XRD of $FeO_x@C_{500\ ^\circ C}$ and $FeO_x@C_{600\ ^\circ C}$ microrods and their PS pollutant removal

Figure S4. XPS spectra of MIL-88(Fe) and survey spectra of $FeO_x@C_{450^\circ C}$.

Figure S5. Nitrogen adsorption–desorption isotherms MIL-88(Fe)

Figure S6. FESEM images of PS nanobeads before and after adsorption on MILBots

Figure S7. Adsorption studies of nanoplastics. Pseudo-second-order kinetics and Langmuir isotherm plots of MILBots.

Figure S8. Removal efficiency of MILBots at different acidic and basic conditions.

Figure S9. Influence of pH on the zeta potential of MILBots and FTIR spectra of MILBots before and after PS beads adsorption.

Figure S10. Removal efficiency of MILBots over PS nanoplastics under different harsh conditions.

Figure S11. Pictorial images of the custom-built magnetic setup

Section S1. Isotherms and Kinetics Studies.

Table S1: Comparison of previous studies on nanoplastics capture with different microrobots.

Table S2. Parameters of pseudo-first-order and second-order kinetic models.

Table S3. Isotherm parameters for PS bead adsorption on MILBots

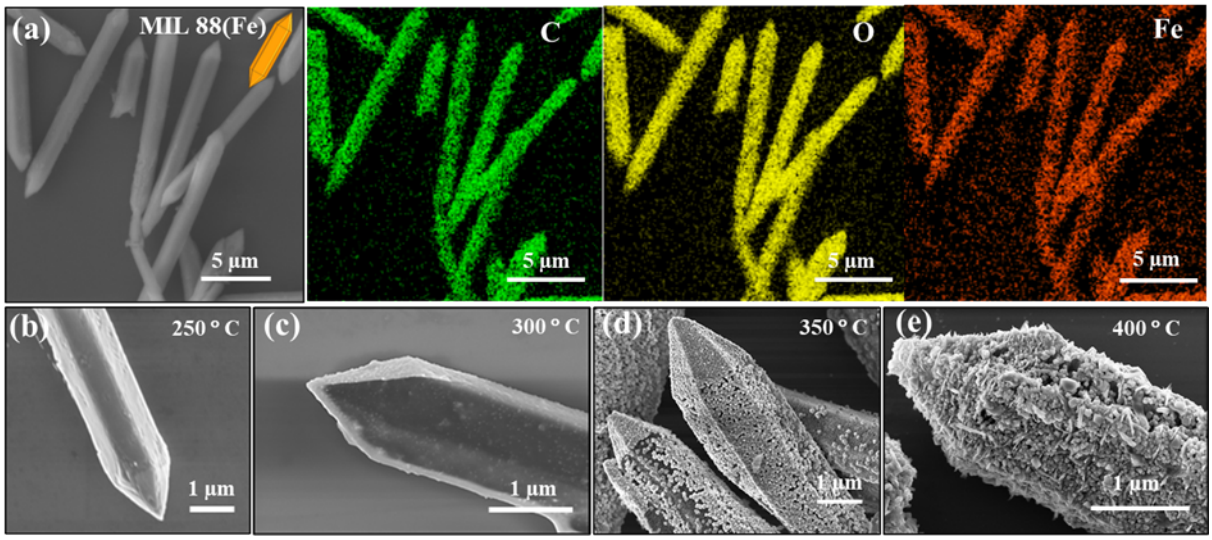

Figure S1. Morphological characterization of Fe-MOF and its derivatives. (a) FESEM and elemental mapping images of MIL-88(Fe). (b)-(e) FESEM images of Fe-MOF derived FeOx@C microrods treated at different temperatures, i.e., 250 ºC, 300 ºC, 350 ºC, and 400 ºC.

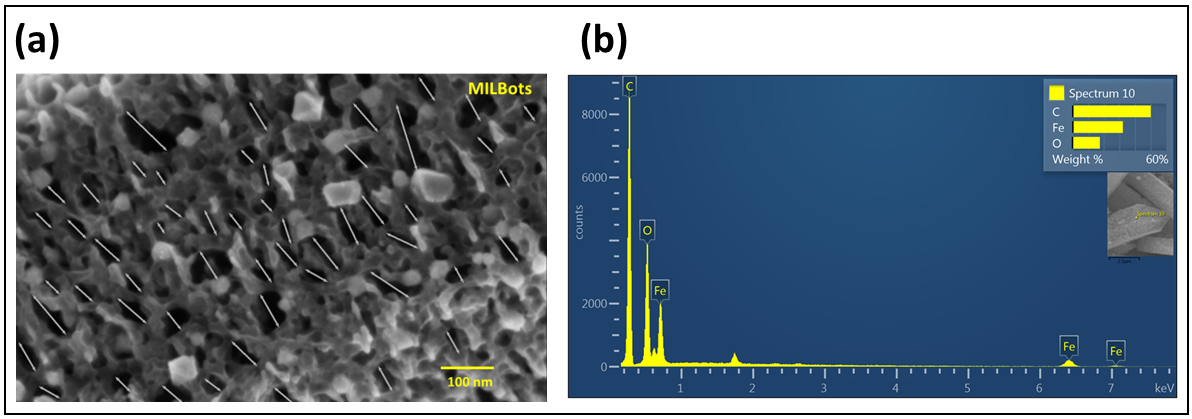

Figure S2. (a) FESEM morphological evidence of pore size distribution on the surface of MILBots. The scale bar is 100 nm. (b) EDS point analysis for a representative $FeO_x@C_{450^{\circ}C}$ (MILBots). The inset shows the location for the analysis, and

Higher calcination temperatures. The carbonisation study was extended to higher temperatures (500 and 600 °C) to further confirm the MILBots surface chemistry. The results show that increasing the temperature leads to partial microrod structural collapse (Figure S3(a-

c)). The rod morphology became agglomerated and disrupted, with an average length of 4.5 µm. Noticeable changes were also observed in the characteristic diffraction peaks of Fe3O4@C500˚C and Fe3O4@C600˚C in the XRD patterns. Despite the higher degree of carbonisation, this results in improved PS nanobeads adsorption efficiency of 88% and 91% for FeOx@C500 ˚C and FeOx@C600 ˚C, respectively (Figure S3(d)) because of its carbon skeleton structure.

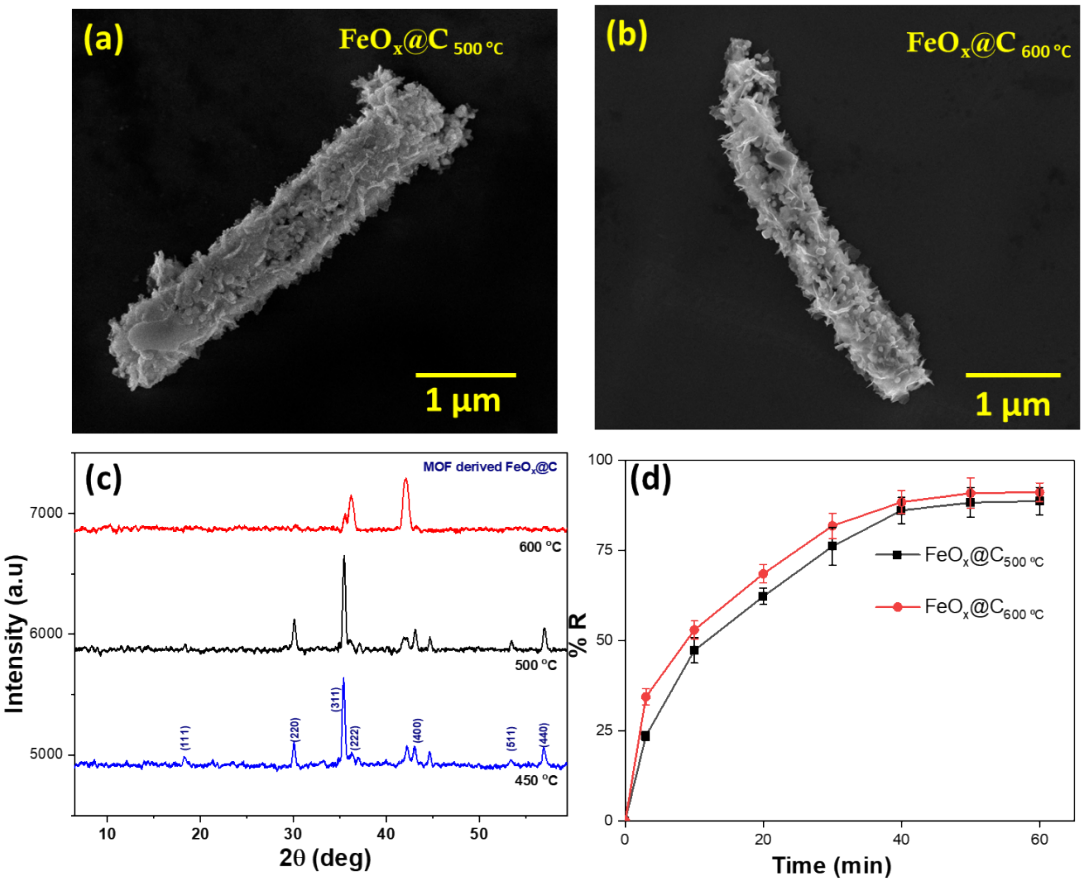

Figure S3. Higher carbonisation microrods and its performance. (a,b) FESEM images of $FeO_x@C_{500\ ^\circ C}$ and $FeO_x@C_{600\ ^\circ C}$ microrods, (c) XRD pattern (d) Removal efficiency of microrods to PS nanobeads.

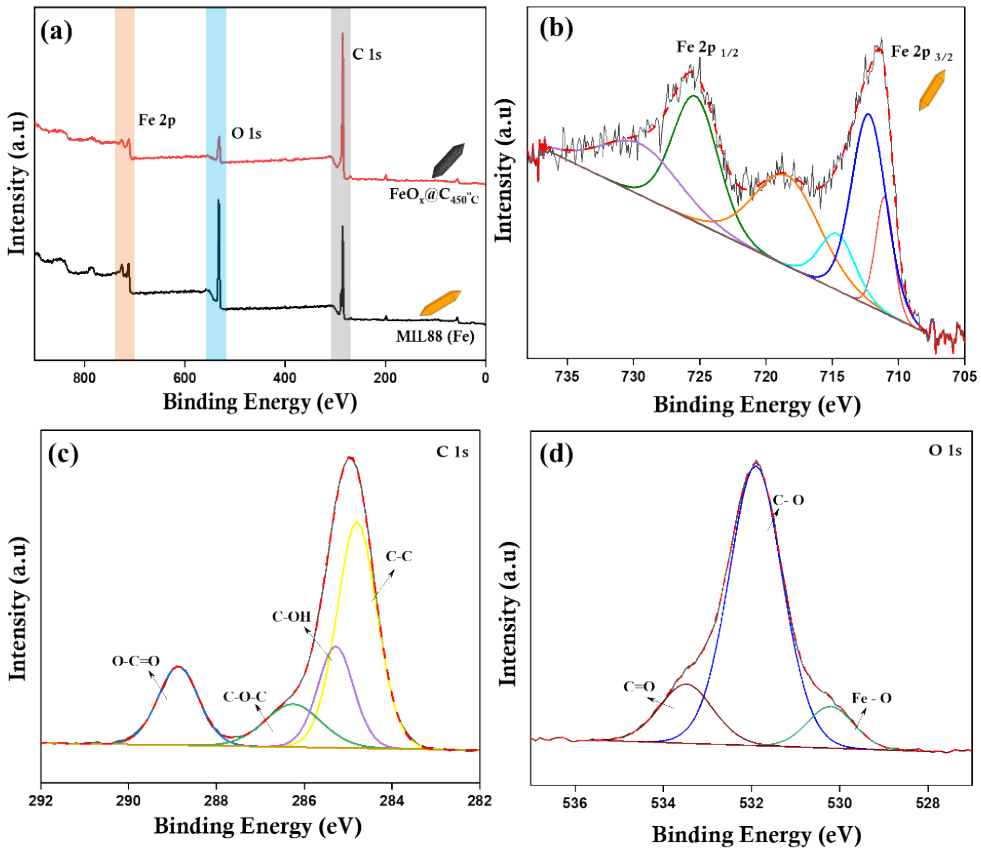

Figure S4. Surface analysis of Fe-MOF. (a) XPS survey spectra of MIL-88(Fe) and $FeO_x@C_{450^{\circ}C}$. (b)-(d) High resolution XPS spectra of MIL-88(Fe) for Fe 2p, C 1s, and O 1s, respectively.

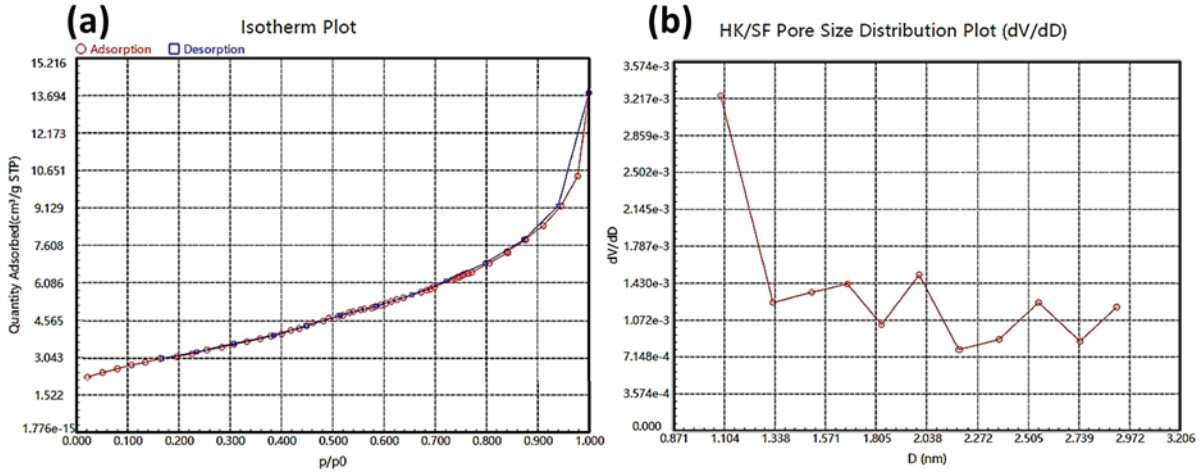

Figure S5. (a) Nitrogen adsorption–desorption isotherms and (b) pore size distributions of MIL 88(Fe).

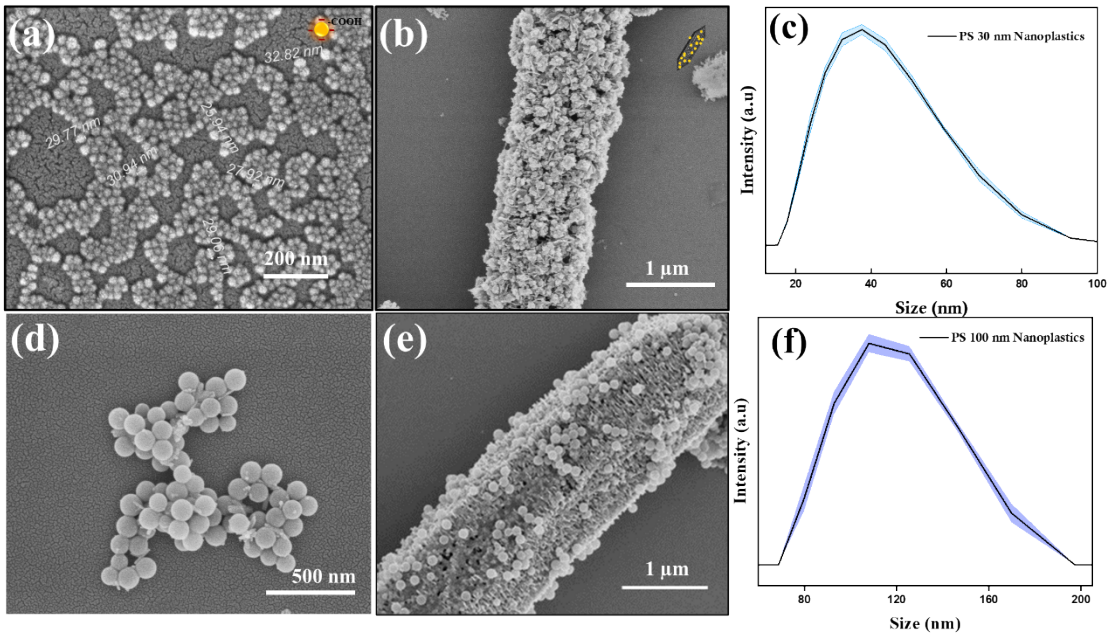

Figure S6. Capture of nanoplastics. (a) FESEM images of carboxylate polystyrene beads having 30 nm diameter and (b) the adsorbed beads on MILBots. (c) Size distribution of the polystyrene beads. (d) FESEM images of polystyrene beads having 100 nm diameter and (e) the adsorbed beads on MILBots. (f) Size distribution of the polystyrene beads.

Table S1: Comparison of previous studies on nanoplastics capture using different microrobots.

S.No	*Materials*	*Nanoplastics*	*Locomotion*	*Size of the micro/nanorobot*	*Average Speed (µm /s)*	*Adsorption in 10 min*	*Removal Efficiency*	*Max. Adsorption capacity (mg/g)*	*Reusability*	*Ref*
1	Polymeric amine-modified dynabead microrobot	PS 1 µm	Magnetic	2.8 µm	30	25%	70%	-	50%	[1]
2	GaIn-Fe liquid metal microrobots	PS 30 nm	Magnetic	30 µm	150	26%	80%	-	72 %	[2]
3	Pt single atom TiO_2-Nanotube	PS 4.8 µm	UV irradiation and H_2O_2	4 µm	2.6	-	-	-	-	[3]
4	Algae surface with Fe_3O_4 nanoparticles	PS 100 nm	Magnetic	5 µm	35	50 %	~90 %	-	80 %	[4]
5	2D MOF nano piller	PS 1 -µm	-	30 nm	-	90 %	100 %	-	81 %	[5]
6	Fe_3O_4 NP	PS	-	-	-	20 %	95.45%	454.5	-	[6]
7	Fe-modified Fly ash material	PS	-	-	-	20%	90%	89.9	84 %	[7]
8	MILBots	PS 30 nm	Magnetic	13 µm	28	~48 %	78%	229	~75%	**Present work**

Section S1. Isotherms and Kinetics Studies. Batch experiments were carried out by adding 50 mg/L of the adsorbent to a test tube containing different initial PS nanoplastics concentrations (5 to 20 mg/L). The tube was maintained under 3 mT and 20 Hz magnetic field[6] for magnetic motion for 60 min. Once the adsorption process reached equilibrium, at a particular interval, the adsorbent was removed by magnetic separation, and the supernatant was analysed by spectrofluorometer (Jasco FP-8300) to check the residual carboxylated PS nanoplastic concentrations. The type of adsorption on the adsorbent is described by the Langmuir and Freundlich adsorption isotherm models[8]. The Langmuir isotherm refers to homogeneous monolayer adsorption, in which adsorption can occur at the active surface sites that are identical and equivalent. The linear and nonlinear forms of the equations are written as,

$$\frac{C_e}{q_e} = \frac{1}{q_m K_L} + \frac{C_e}{q_m} \qquad (6)$$

where q_e and q_{m} are the equilibrium adsorption capacity and maximum adsorption capacity (mg/g) of the adsorbate, respectively; C_e (mg/L) is the concentration of adsorbate at equilibrium, and K_L (L/g) is a constant related to the affinity between the adsorbent and adsorbate.

The Freundlich isotherm model is an empirical equation commonly used to describe the adsorption characteristics of a heterogeneous surface and can be applied to multilayer adsorption of an adsorbate on the surface of an adsorbent. The isotherm equations can be expressed as,

$$\ln q_e = \ln K_F + \left(\frac{1}{n}\right) \ln C_e \qquad (7)$$

Where, q_e (mg/g), C_e (mg/L) are the same as mentioned in the Langmuir model. n is the heterogeneity coefficient, and K_F (L/g) is the characteristic constant related to the multilayer adsorption capacity.

The kinetic experiments were carried out by adding 50 mg/L of the adsorbent to a test tube containing 2 mL of 10 mg/L PS solution. The adsorbent was then removed by an external magnet after the process and the supernatant was analyzed by spectrofluorometer to check the residual PS concentrations. The kinetics of present adsorption studies at different time intervals were investigated by pseudo-first-order and pseudo-second-order kinetic models. Processes such as the rate of reaction and the mass transfer were determined by applying the pseudo-first-order model[7]. The pseudo-first-order rate equation can be expressed as:

$$\log (q_e - q_t) = \log q_e - \left(\frac{k_1}{2.303}\right)t \qquad (8)$$

The pseudo-second-order kinetic model is represented by the following equation:

$$\frac{t}{q_t} = \frac{1}{k_2 q_e^2} + \frac{t}{q_e} \qquad (9)$$

Where, q_e is the equilibrium removal capacity and q_t is the removal capacity (mg/g) at time t, respectively, and k_1 is the pseudo-first-order rate constant (1/min) and k_2 is the pseudo-second-order rate constant (g/mg min).

The effects of adsorbent dosage and pH on the sorption of conditions were carried out by adding different initial (10-100 mg/L) amounts of the adsorbent to a test tube containing 2 mL of 10 mg/L PS solution. After the adsorption process for 60 min, the adsorbent was then removed by an external magnet and the supernatant was analyzed by spectrofluorometer to check the residual PS concentrations. The pH-dependent studies were carried out by adding 50 mg/L of the adsorbent to a test tube containing 2 mL of 10 mg/L PS solution. The acidic and basic pH was maintained using diluted HCl and NaOH solution. The adsorbent was then removed by an external magnet after the process and the supernatant was analyzed by spectrofluorometer to check the residual PS concentrations.

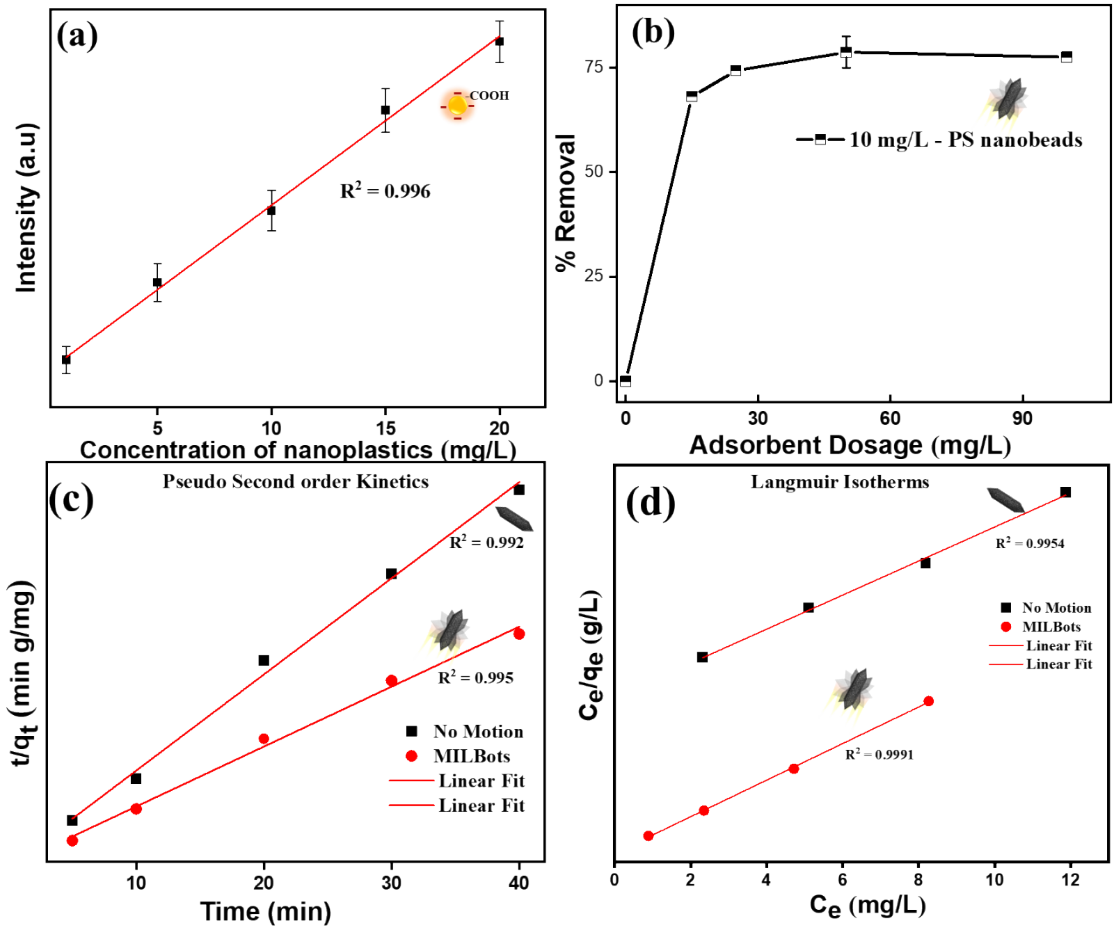

Figure S7. Adsorption studies of nanoplastics: (a) Calibration curve for the concentration of nanoplastics versus photoluminescence intensity. (b) The removal efficiency of MILBots with

different dosages of PS beads at pH 7. (c) and (d) Pseudo-second order kinetics and Langmuir isotherms plots of MILBots without motion and with magnetic motion.

Table S2. Parameters of pseudo-first-order and second-order kinetic models. The values are for a PS concentration of 10 mg/L as calculated from the plot in *Figure S7c.*

Kinetics	**Parameters**	**Adsorption systems MILBots**
Experimental value	q_e,exp (mg g^{-1})	**229.4**
Pseudo-first-order	k_1 (min^{-1})	0.08
	q_e,cal(mg g^{-1})	203.9
	R^2	0.818
Pseudo-second-order	k_2 (g mg^{-1} min^{-1})	0.0002
	q_e,cal (mg g^{-1})	233.1
	R^2	0.995

Table S3. Isotherm parameters for PS bead adsorption on MILBots as calculated from the plots in *Figure S7d.*

Isotherm	**Parameters**	**Adsorption systems MILBots**
Langmuir	q_{max} (mg g^{-1})	454.54
	k_L (L mg^{-1})	0.43
	R^2	0.9991
Freundlich	k_F (L mg^{-1})	139.34
	n_f	2.095
	R^2	0.9662

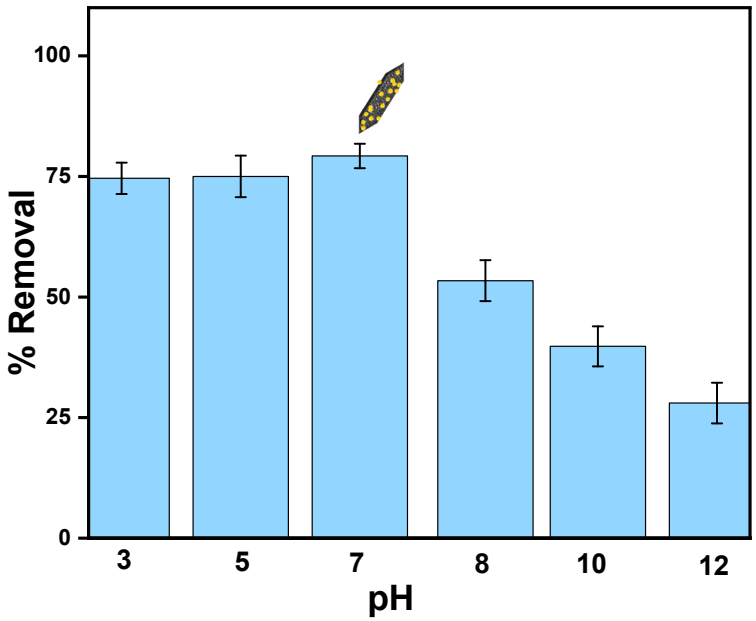

Figure S8. Removal efficiency of MILBots at different acidic and basic conditions.

Figure S8 shows that the adsorption of PS beads sustained with the decrease of solution pH. The results might indicate that the surface of MILBots can be protonated when the acidic pH. A positive surface at a lower pH can lead to PS beads molecule sorb on MILBots surface than basic pH.

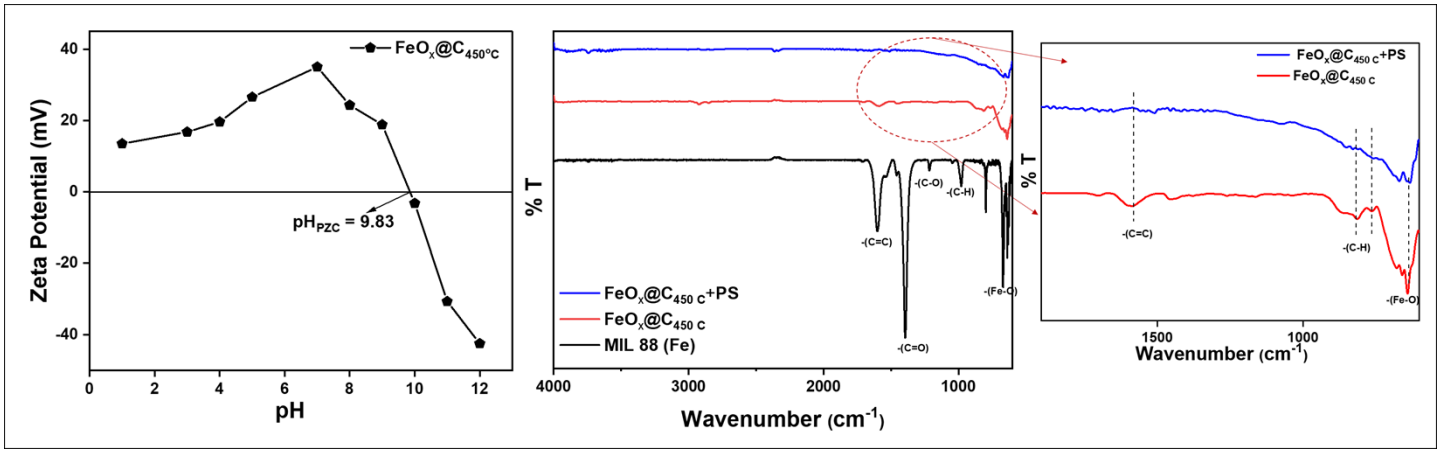

Figure S9. (a) Influence of pH on the zeta potential of MILBots. **(b)** FTIR spectra of MIL88(Fe) and MILBots before and after PS beads adsorption.

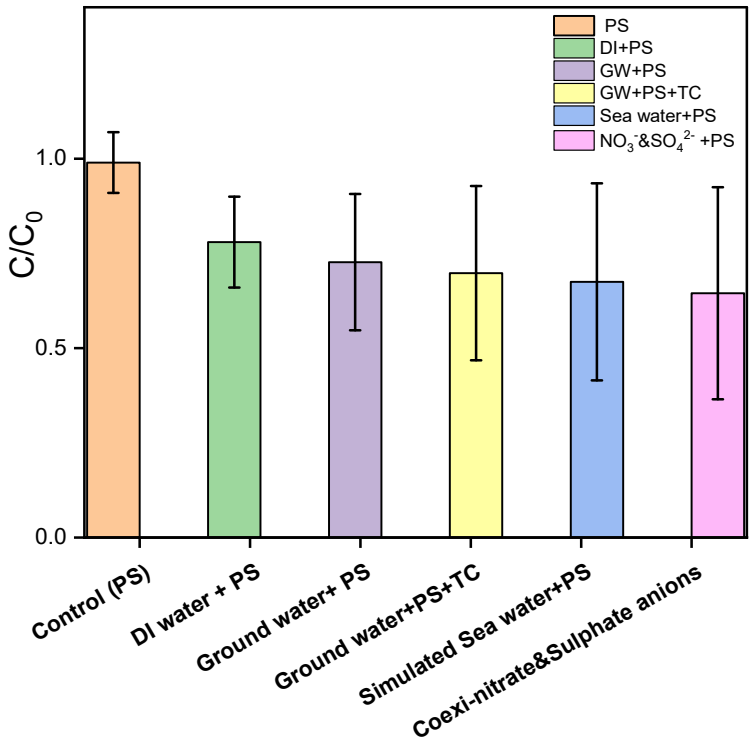

Figure S10. Removal efficiency of MILBots over PS nanoplastics under different harsh conditions.

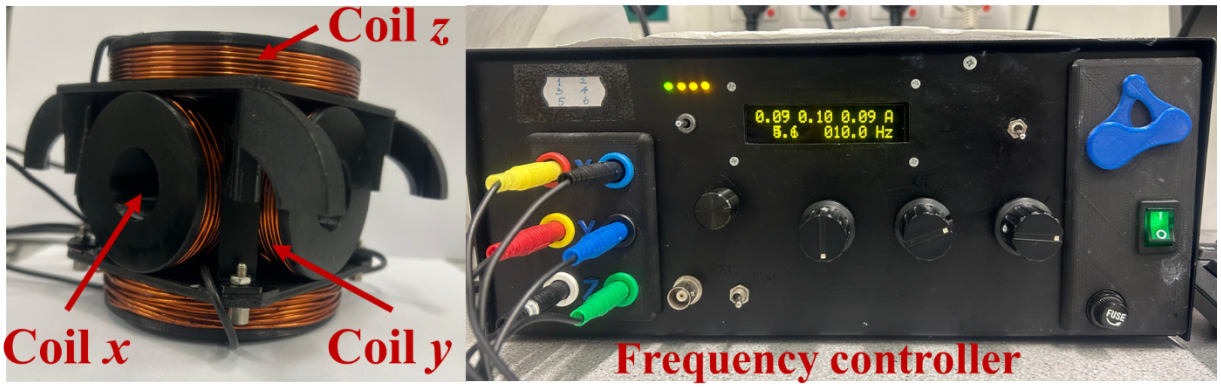

Figure S11. Pictorial images of the custom-built magnetic setup utilised during the experiments.

References

(1) Ussia, M.; Urso, M.; Oral, C. M.; Peng, X.; Pumera, M. Magnetic Microrobot Swarms with Polymeric Hands Catching Bacteria and Microplastics in Water. *ACS Nano* 2024, *18* (20), 13171-13183. DOI: 10.1021/acsnano.4c02115.

(2) Wu, X.; Peng, X.; Ren, L.; Guan, J.; Pumera, M. Reconfigurable Magnetic Liquid Metal Microrobots: A Regenerable Solution for the Capture and Removal of Micro/Nanoplastics. *Advanced Functional Materials* 2024, *34* (51), 2410167. DOI: https://doi.org/10.1002/adfm.202410167.

(3) Jancik-Prochazkova, A.; Kmentova, H.; Ju, X.; Kment, S.; Zboril, R.; Pumera, M. Precision Engineering of Nanorobots: Toward Single Atom Decoration and Defect Control for Enhanced Microplastic Capture. *Advanced Functional Materials* 2024, *34* (38), 2402567. DOI: https://doi.org/10.1002/adfm.202402567.

(4) Peng, X.; Urso, M.; Kolackova, M.; Huska, D.; Pumera, M. Biohybrid Magnetically Driven Microrobots for Sustainable Removal of Micro/Nanoplastics from the Aquatic Environment. *Advanced Functional Materials* 2024, *34* (3), 2307477. DOI: https://doi.org/10.1002/adfm.202307477.

(5) Haris, M.; Khan, M. W.; Zavabeti, A.; Mahmood, N.; Eshtiaghi, N. Self-assembly of C@FeO nanopillars on 2D-MOF for simultaneous removal of microplastic and dissolved contaminants from water. *Chemical Engineering Journal* 2023, *455*, 140390. DOI: https://doi.org/10.1016/j.cej.2022.140390.

(6)Matar, G. H., Dikbas, C., & Andac, M. Efficient magnetic adsorption of polystyrene nanoplastic from aqueous solutions by eco-friendly Fe3O4 nanoparticles: Removal, kinetic and isotherm modeling studies. *Journal of Environmental Health Science and Engineering*, 2024, *23*(1), 4. DOI: https://doi.org/10.1007/s40201-024-00929-7.

(7)Zhao, H., Huang, X., Wang, L., Zhao, X., Yan, F., Yang, Y., ... & Ji, P. Removal of polystyrene nanoplastics from aqueous solutions using a novel magnetic material: Adsorbability, mechanism, and reusability. *Chemical Engineering Journal*, 2022, *430*, 133122. DOI: https://doi.org/10.1016/j.cej.2021.133122Get rights and content

(8)Minitha, C. R.; Suresh, R.; Maity, U. K.; Haldorai, Y.; Subramaniam, V.; Manoravi, P.; Joseph, M.; Rajendra Kumar, R. T. Magnetite Nanoparticle Decorated Reduced Graphene Oxide Composite as an Efficient and Recoverable Adsorbent for the Removal of Cesium and Strontium Ions. *Industrial & Engineering Chemistry Research* 2018, *57* (4), 1225-1232. DOI: 10.1021/acs.iecr.7b05340.